Making Ceramic Membranes Used in Redox Flow Batteries with Sol-gel Process

Canfeng Wei

A thesis

submitted in partial fulfillment of the

requirements for the degree of

Master of Science in Chemical Engineering

University of Washington

2018

Committee:

Lilo D. Pozzo

John C. Berg

Program Authorized to Offer Degree:

Department of Chemical Engineering

University of Washington

Abstract

Making Ceramic Membranes Used in Redox Flow Batteries with Sol-gel Process

Canfeng Wei

Chair of the Supervisory Committee:

Lilo D. Pozzo

Department of Chemical Engineering

To increase the amount of renewable energy utilized in electrical grids, large- scale batteries are required. Redox flow batteries (RFBs) are promising batteries. However, the high cost of electrolytes and membranes impede the application of RFBs. It is worth exploring a new membrane with inexpensive material and simple process. The goals of this project are to explore a new anion exchange membrane using sol-gel process and to find the ceramic materials can be used as the membrane materials of alkaline-based organic RFBs. The membranes were prepared by coating silica paper with titania. After sintering, titania membranes survived in 3 M HCl but showed worse permeability performance than Nafion membranes. Thus, titania might not be the proper membrane material of anion exchange membranes. The cellulose paper coated with

Ludox® CL was stable in 1 KOH. Therefore, alumina might be the proper membrane material utilized in alkaline-based organic RFBs.

TABLE OF CONTENTS

LIST OF FIGURES

LIST OF TABLES

ACKNOWLEDGEMENTS

I would first like to express my gratitude to my thesis advisor Prof. Lilo D. Pozzo. Prof. Pozzo always patiently guide me and give me helpful suggestion in this project. Besides advisor, I would like to thank to my committee: Prof. John Berg. I would also like to thank Dr. Greg Newbloom for SEM images. I am grateful to every member in Pozzo's lab, who provided lots of help throughout this project. Special thanks should be given to Dr. David S. Li, Dr. Yuyin Xi, and Yi-Ting Lee for scattering data obtained from Argonne National Laboratory. Finally, I would like to thank my parents for providing support and encouragement throughout my study.

Chapter 1. INTRODUCTION

Most of electricity generation in the world comes from fossil fuel, and the other comes from nuclear and hydroelectric power generation [1]. Fossil fuel is nonrenewable energy, and the combustion of fossil fuel causes gas emission problems. Increasing the amount of renewable energy sources utilized in electricity generation can alleviate the problem. However, renewable energy sources depend on climate. They are unpredictable, so they cannot provide power steadily and continually. For example, a solar cell produces energy at day while it provides no energy at night when electricity demand is large. Therefore, we need batteries to store spare energy at peak output and to release energy when production rate is lower than consumption rate.

1.1 REDOX FLOW BATTERIES

Redox Flow batteries (RFBs) is one type of promising batteries. RFBs consist of two storage tanks and a reaction cell in the center. Electrolytes are pumped from the tank to the cell. During discharging, the anolyte loses electrons and the catholyte gains electrons. Ion exchange occurs at the membrane in the cell to maintain charge neutrality. Since an electron current loop forms, batteries can run external loads. RFBs have advantages of large energy capacity and simple recharge process. Figure 1.1 shows the structure of a RFB.

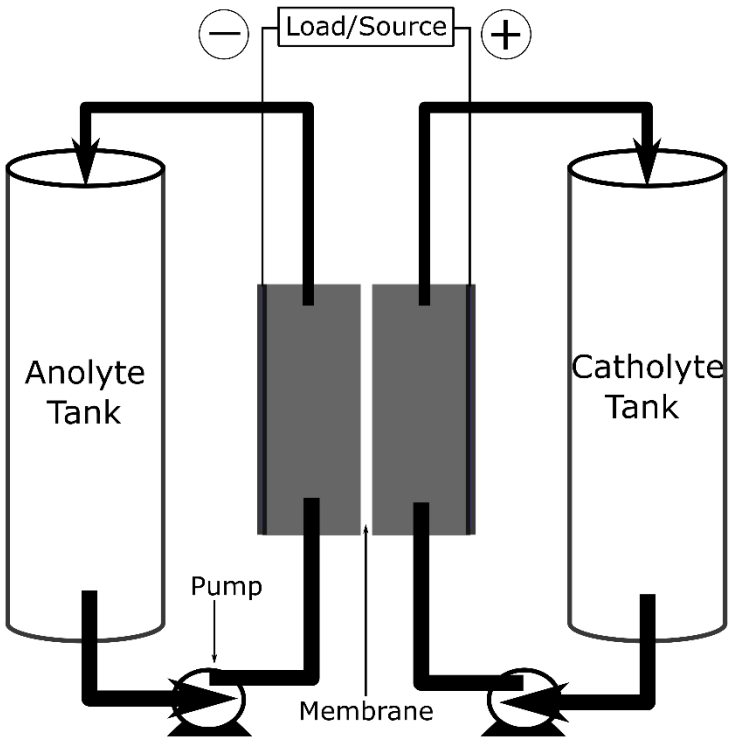

Figure 1.1: The schematic of a redox flow battery.

The all-vanadium redox battery (VRB) is one type of RFBs. In VRBs, during charging, $VO^{2+}$is oxidized to VO_2^+, and V^{3+} is reduced to V^{2+}. The process is reversed during discharging. Hydrogen ions cross through the membrane to maintain charge neutrality. The two electrolyte streams in VRBs are solutions of the same element with different oxidation states. Therefore, the crossover of electrolyte would only cause efficiency loss but would not result in irreversible electrolyte degradation [1]. Thus, VRBs are widely utilized and receive the most attention. The capital cost target of RFBs is \$150-\$200/kWh in 2020 [2], while the capital cost of the VRB system in base case would be about \$380/kWh [3]. Expensive vanadium resources and high priced Nafion membranes are two factors that lead to the high cost of VRBs [4]. The low energy density of VRBs caused by the low solubility of vanadium ions in the electrolyte also impedes the application of VRBs [5].

Iron also has three different oxidation states, so it can also be used to make an all-iron flow battery. Compared with VRBs, the use of iron solutions as electrolytes shows advantages of lower cost and better environmental safety because iron is the most abundant element on Earth, and the electrolyte is nonflammable and nonhazardous. In an all-iron flow battery, during charging, Fe^{2+} is reduced to Fe^{0} in the negative electrode, and Fe^{2+} is oxidized to Fe^{3+} in the positive electrode. Chloride ions are the charge-balancing ions that pass through the membrane. VRBs and all-iron flow batteries both work under highly acidic conditions, where pH is about 0.

Organic redox flow batteries (ORFBs) are RFBs using organic materials as active materials. Using organic materials as catholyte or anolyte has advantages of diverse molecular moieties, wide range of redox potentials, and low material cost [5]. ORFBs can be classified into aqueous ORFBs and non-aqueous ORFBs. In aqueous ORFBs, the organic materials can dissolve in water-based electrolytes like the acid-based 9,10-anthraquinone-2,7-disulphonic acid (AQDS)/bromine ORFB and the alkaline-based alloxazine 7/8-carboxylic acid (ACA)/ ferrocyanide ORFB.

The ion exchange membrane (IEM) is a critical component of RFBs. A good IEM should prevent the crossover of active species in the electrolyte but also allow the transfer of charge balancing ions like H^+ and Cl^-. Nafion is the most widely used membrane material. Nafion is a fluorocarbon polymer, which consists of a hydrophobic Teflon-like backbone with hydrophilic side chains that are decorated with sulfonic acid groups [6]. Nafion is utilized as membrane material because of its high proton and sodium conductivities, and it has a conduction mechanism that includes both ion hopping and vehicular modalities [1]. The chemical structure of Nafion is shown below. Nafion has high cation conductivity and blocks other ions, so it may show bad anion exchange performance in the all-iron flow battery where chloride ions act as charge-balancing ions. The proton conductivity of Nafion membranes also becomes worse under basic conditions,

which may affect the performance of alkaline-based ORFBs. Another significant problem of Nafion is its high price. Nafion can account for up to 40% of the total cost of a RFB cell stack [6], which impedes commercialization. Thus, it is worth studying a new anion exchange membrane with inexpensive materials, better performance and simpler processing.

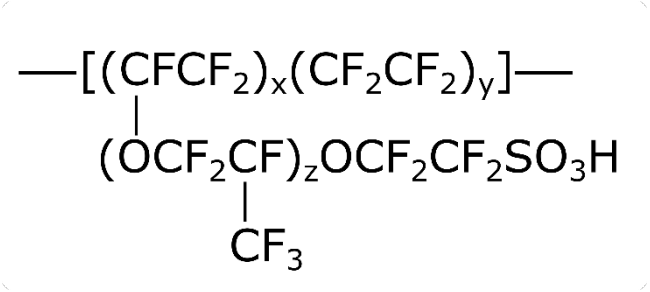

Figure 1.2: The chemical structure of Nafion.

1.2 Sol-gel Process and Ceramic Membranes

Nafion/SiO_2 hybrid membranes prepared by in situ sol-gel method shows much lower permeability of vanadium than Nafion membranes because of the polar clusters[7]. Silica gel can be a promising membrane material to replace Nafion. Silica is much cheaper than Nafion, and it can be easily prepared by the sol-gel method. The sol-gel process is a method to synthesize an inorganic network by a chemical reaction in solution[8]. It can produce colloidal gel with high levels of chemical homogeneity[9]. The sol-gel method is usually used for fabrication of ceramic materials, such as silica, titania, and alumina. The silica membranes studied in the Pozzo group show Fe^{3+} permeability performance that is close to Nafion membranes [10]. However, silica membranes are not expected to be good materials for anion exchange membranes.

Three different types of materials were compared to find the appropriate material used for anion exchange membranes. Table 1.1 shows the properties of these ceramic materials. When metal oxide is hydroxylated in moisture environment, the surface could carry positive charges or

negative charges. When the pH of solutions is lower than the point of zero charge (PZC), the material would carry positive charges. Silica has PZC around 2, which means that silica will carry negative charges under most acidic conditions. The negative surface charges aid in the transport of protons. However, in all-iron flow batteries, anion exchange membranes are preferred. Based on the properties, the preparation method, and the chemical cost of these ceramic materials, titanium dioxide was picked as the membrane material of anion exchange membranes. Titania has advantages of proper PZC, simple preparation method, and low chemical cost. The goals of this project are to explore a new anion exchange membrane using sol-gel process and to find ceramic materials that can be used as the membrane materials of alkaline-based ORFBs.

Table 1.1: The Comparison among Some Ceramic Materials

	TiO_2	Al_2O_3	SiO_2
Point of zero charge (PZC) (pH)	6-7	8-9	2-3
Positive surface potential range (pH)	<6	<8	<2
Chemical stability in HCl	Insoluble	React with hot dilute HCl	Insoluble
Chemical stability (pH) [11]	--	3<pH<13	2<pH<8
The preparation method of ceramic materials	Hydrolyze titanium tetraisopropoxide (TTIP) in ethanol [12].	Hydrolyze aluminum s-butoxide in sec-butyl alcohol [13].	Hydrolyze tetraethyl orthosilicate (TEOS) [10].
Chemicals involved	TTIP, HCl, ethanol and DI water	Aluminum s-butoxide, sec-butyl alcohol, and glacial acetic acid.	TEOS and polystyrene sulfonic acid
Cost of chemicals	~$43/100 g	~$65/ 100 g	~$57/ 100g

Chapter 2. MATERIALS AND METHODS

The chemicals used in the membrane preparation were titanium tetraisopropoxide (TTIP), tetraethyl orthosilicate (TEOS), Ludox® CL, 3 M hydrochloric acid, DI water, and pure ethanol (EtOH). Ludox® CL is the colloidal silica particle coated with a layer of alumina. 97% TTIP, 99% TEOS, and Ludox® CL (30wt.% suspension in water) were obtained from Sigma-Aldrich Corporation, and pure ethanol 200 proof was from Decon Laboratories, Inc. Other chemicals involved were 98% iron (III) chloride hexahydrate (Sigma-Aldrich Corporation) and 98% aluminum chloride hexahydrate (Sigma-Aldrich Corporation).

2.1 THE PREPARATION METHODS OF MEMBRANES

There were two types of membranes made in the experiments, which are titania membranes and the membranes made from Ludox® CL and ceramic materials (Ludox membranes).

2.1.1 *The Preparation of Titania Membranes*

The hydrolysis of TTIP was described by Marc, Mary, and Qunyin [12]. In their paper, titania sol-gel solutions were prepared by hydrolyzing TTIP with small amount of water in ethanol, and the pH needed to be adjusted to prevent TiO_2 from precipitating. Partially hydrolyzed products are soluble in ethanol and form polymeric chains through the condensation of oxygen bridges. The sol-gel reactions are shown below

$$Ti(OR)_4 + xH_2O \rightarrow Ti(OH)_x(OR)_{4-x} + xHOR \quad (2.1)$$

$$Ti(OR)_y(OH)_x \rightarrow TiO_z(OR)_{y_1}(OH)_{x_1} + (y - y_1)RH \quad (2.2)$$

where $x < 4$, $x_1 < x$, $y_1 < y$, $z = [4 - (x_1 + y_1)]/2$, R is the alkyl group, and z is the number of oxygen bridges formed per titanium atom [12].

The chemicals were mixed in the order of ethanol, HCl, TTIP, and water. The following H_2O:TTIP:EtOH mass ratios of 1:29:18, 1:24:23, and 1:14:32 were utilized. The compositions mentioned in this dissertation are all based on mass, and the percentages of ethanol in sol-gel solutions are omitted when the compositions are mentioned in the figures. TEOS can be hydrolyzed to form silica as Equation 2.3 shows.

$$Si(OR)_4 + H_2O \rightleftarrows Si(OR)_3 + ROH \tag{2.3}$$

where R the is alkyl group [14]. The silica membranes made from Pozzo's group show a more uniform xerogel film. Silica might provide stronger resistance to the tensile stress causing cracks. Thus, silica was added in. Sol-gel solutions could also be prepared with TEOS:TTIP:EtOH mass ratios of 1:21:26, 1:17:26, and 1:10:26. TEOS and TTIP will be hydrolyzed with water in air. The chemicals were mixed in the order of EtOH, TTIP, and TEOS.

Circular silica paper (1 μm nominal pore size, 330 μm thickness, and 14 mm diameter) were coated by dipping the paper in the sol-gel solution for about two minutes. The paper was coated three times. The time interval between two coatings were about ten minutes so that the surface was roughly dry. The coated paper was naturally dried out in the fume hood for about 24 hours after final coating. The membranes were sent to a F6030C furnace from Thermo Scientific for sintering. The furnace was heated up to 50 ℃ below the target temperature at the speed of 5 ℃/min, and then the temperature increased to the target temperature at the speed of 1 ℃/min. The membrane was sintered at the target temperature for 2 hours and then naturally cooled down to room temperature. The membrane was sintered at three different target temperatures, which are 250℃, 350℃, and 450℃.

A heat press with temperature about 325°F was utilized to melt SIBS polymer (Kraton-D 1170) into the membrane edges to form a seal for installation. The melting process took about 30

seconds, and a polymer edge was added to the membrane. 50 µL of toluene was dropped to the boundary between the membrane and the edge to let the edge completely seal the membrane. The membrane was dried out for a day after this. The membrane with the edge was used for permeability tests, as it is shown in the picture below.

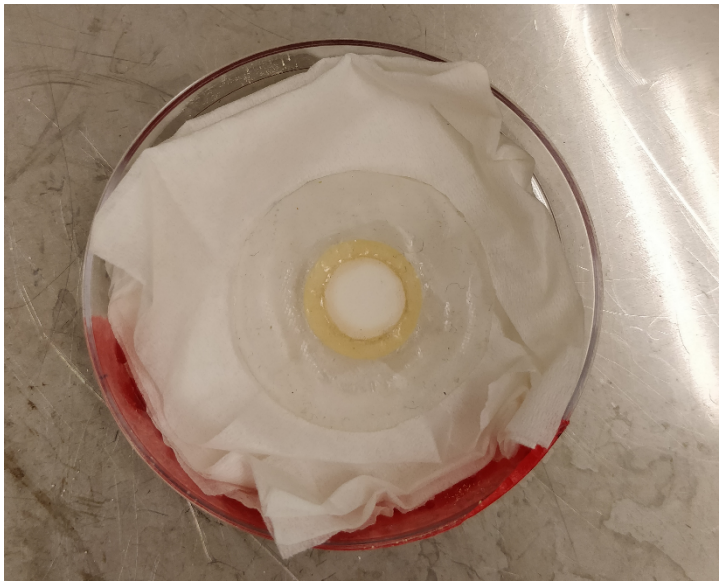

Figure 2.1: The titania membrane with a polymer edge.

2.1.2 *The Preparation of Ludox® CL Membranes*

Ludox® CL are large colloidal silica particles. Large particles might provide stronger resistance to the tensile stress. The membrane is expected to show less cracks if silica paper is coated with Ludox® CL and then coated with sol-gel solutions. Silica paper was dip coated once with Ludox® CL for about 2 minutes. The paper was naturally dried out in fume hood for about 24 hours. After drying, the paper was coated with the titania solution or the silica solution three times. The titania solution had H2O:TTIP:EtOH mass ratio of 1:20:29. The silica solution was prepared by mixing chemicals in the order of ethanol, water, and TEOS. The silica solution with H2O:TEOS:EtOH mass ratio of 1:20:29 was prepared.

2.2 PROPERTY MEASUREMENT

Small Angle X-ray Scattering (SAXS) is an analytical method to determine the structure of nanosized systems in terms of average feature size and shape [15]. The nanostructure of titania membranes were measured at the Argonne National Laboratory Small Angle X-ray Scattering instruments in beamline 9ID at an x-ray energy of 21 keV. The measurements included Ultra Small Angle X-ray Scattering (USAXS), SAXS, and Wide Angle X-ray scattering (WAXS). The scattering times were 180 s, 20 s, and 20 s, for USAXS, SAXS, and WAXS respectively. Data reduction was done with Irena and Nika SAS software, and the scattering data were fit using SasView. Details of fit model are shown in Appendix A. Microstructure information of the membranes were obtained by scanning electron microscope (SEM) (Sirion XL 30).

The permeability of Fe^{3+} was measured to quantify the performance of the membranes. The membranes were soaked in 3 M HCl for a day before permeability tests. 1 M $FeCl_3$ solution was prepared by dissolving iron (III) chloride hexahydrate with 3 M HCl. Similarly, 1 M $AlCl_3$ solution was prepared by dissolving aluminum chloride hexahydrate with 3 M HCl. Permeability cells were assembled as shown in Figure 2.2. 10 ml of each solution was put in to each side, and the membrane was in the center. Time was recorded after the two solutions were added. At time 0, 1 ml of $AlCl_3$ was taken out as a reference, and 1 ml of $AlCl_3$ was refilled. 1 ml of solution was removed from $AlCl_3$ cell, and 1 ml of $AlCl_3$ was refilled after each time interval. The time interval can be 2 min, 5 min or 10 min, which depends on the performance of the membranes. The permeability tests can last about one hour. The solutions removed from the $AlCl_3$ cell were tested by UV-VIS spectrophotometer (Evolution 300), and Fe^{3+} concentrations were obtained using Beer's law. The permeability of Fe^{3+} could be obtained based on how the concentration changed with time. Details of how to calculate the permeability are described in Appendix B.

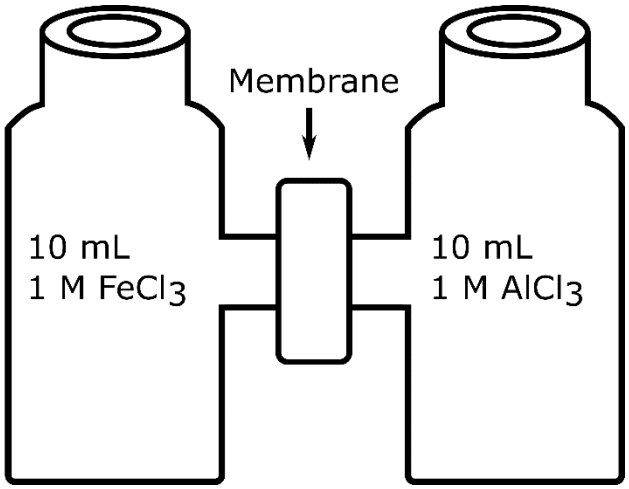

Figure 2.2: The schematic of the permeability cells.

2.3 STABILITY TESTS IN 1 M KOH

Stability tests were performed based on long time immersion in 1 M KOH. Silica will react with concentrated KOH to form silicate salt, so silica paper was replaced with cellulose paper. The cellulose paper with a thickness of 190μm and a pore size of 1 μm was utilized as the substrate in the stability test. Three different samples were prepared. One was the cellulose paper coated with titania sol-gel solution with H2O:TTIP:EtOH mass ratio of 1:20:29. The coating process of the sample was the same as that of titania membranes. The other sample was prepared by dipping cellulose paper in Ludox® CL once for 2 min. The last sample was blank cellulose paper. After coating and drying, the samples were tested by SAXS (Anton Parr SAXSess). The samples were soaked in 1 M KOH for a day after SAXS, and then they were rinsed with DI water. After the samples were completely dry, they were tested again using SAXS.

Chapter 3. RESULTS

3.1 THE STRUCTURE INFORMATION OF TITANIA MEMBRANES

Membranes are sent to SEM to obtain microstructure information. Surface and cross-sectional images are taken for every sample using SEM. Blank silica paper is also tested with SEM, and the results are shown in Figure 3.1.

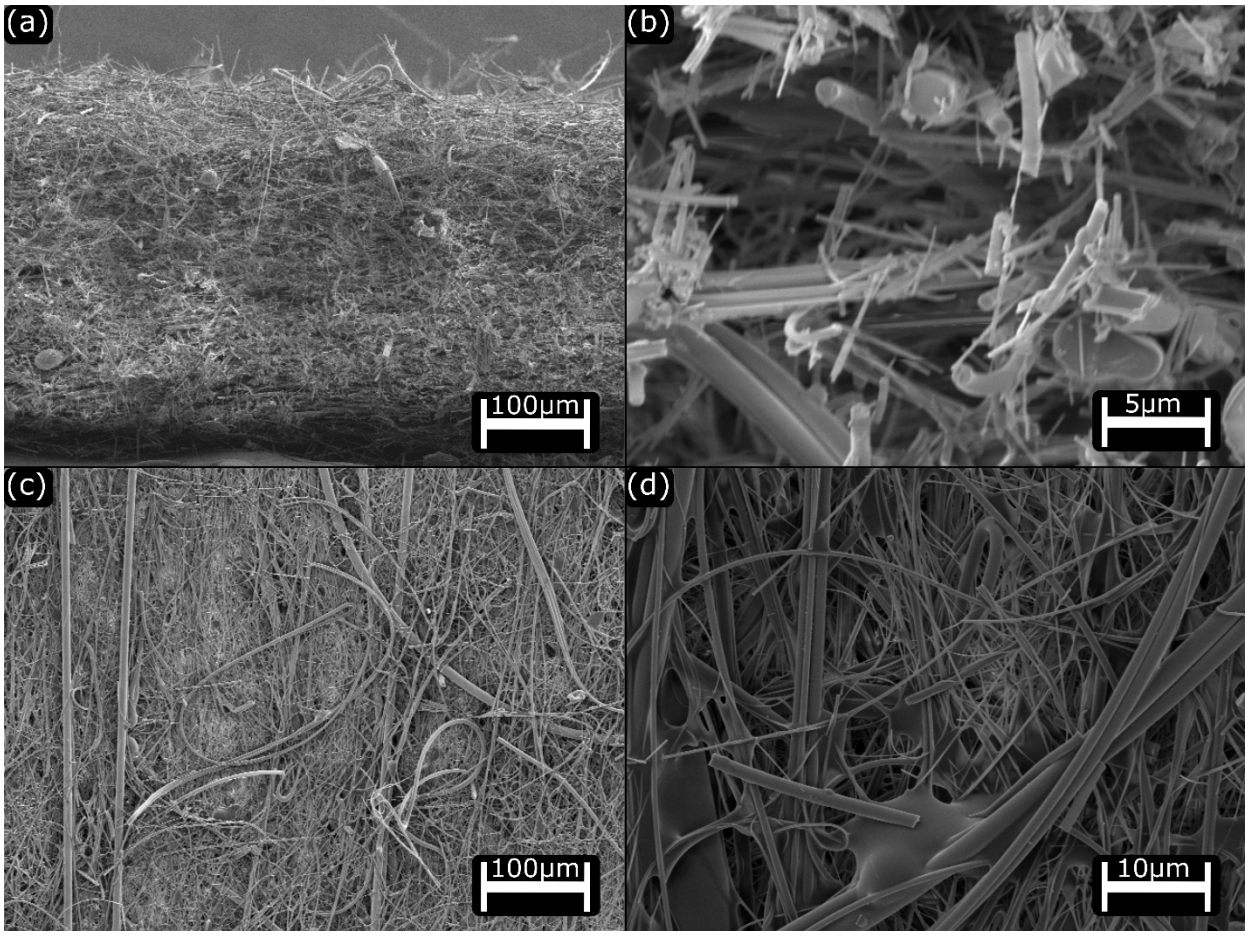

Figure 3.1: The SEM images of blank silica paper. Cross-sectional images in (a) 100 µm scale and in (b) 5 µm scale; Surface images in (c) 100 µm scale and in (d) 10 µm scale.

3.1.1 *The Structure Information of Membranes Made from TTIP and Water*

The SEM images of the membrane made from TTIP and water (TTIP-H_2O membrane) are shown below. A xerogel film forms on the top of the membrane, and there are lots of cracks. The cracks are caused by tensile residual stress due to film densification [16]. Compared with cross-sectional images of silica paper, the membrane shows more compact structures. It means that silica paper is successfully coated with titania sol-gel solutions, and the solutions penetrate silica paper. However, the xerogel network does not form inside the membrane, and it seems that small titania particles aggregate inside the membrane.

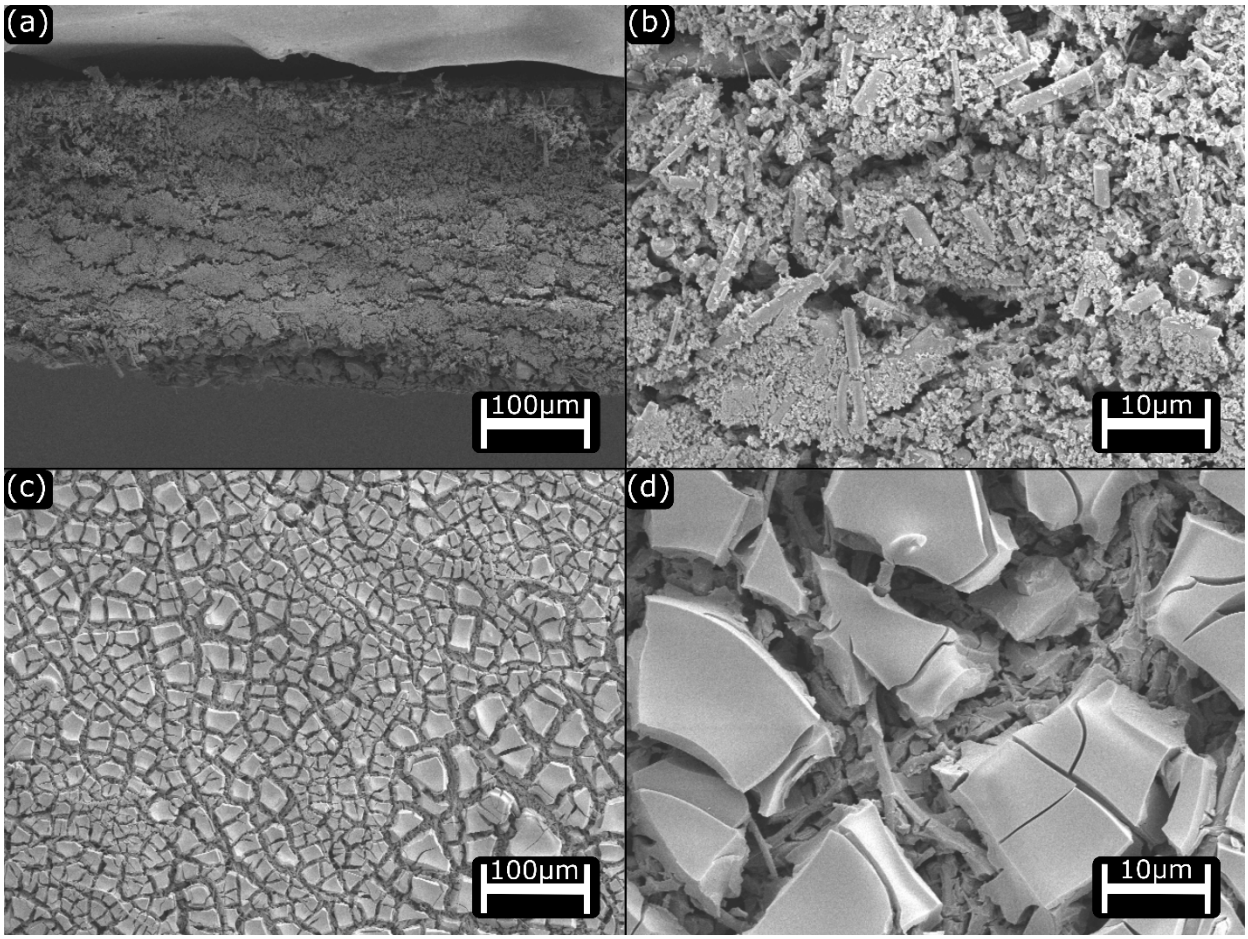

Figure 3.2: The SEM images of the membrane made from 40% TTIP, 2% water and 58% EtOH. Cross-sectional images in (a) 100 µm scale and in (b) 10 µm scale; Surface images in (c) 100 µm scale and in (d) 10 µm scale.

The figure below shows the scattering graphs and their fit of TTIP-H_2O membranes. The details of the fit model are described in Appendix A. Table 3.1 exhibits the fit results of the parameters from fractal model. Interestingly, the membrane with 50% of TTIP and the membrane with 60% of TTIP show similar scattering graphs and fit results. The sol-gel solution might be saturated with TTIP when there is about 50% of TTIP, and the more TTIP added in would not affect the membrane.

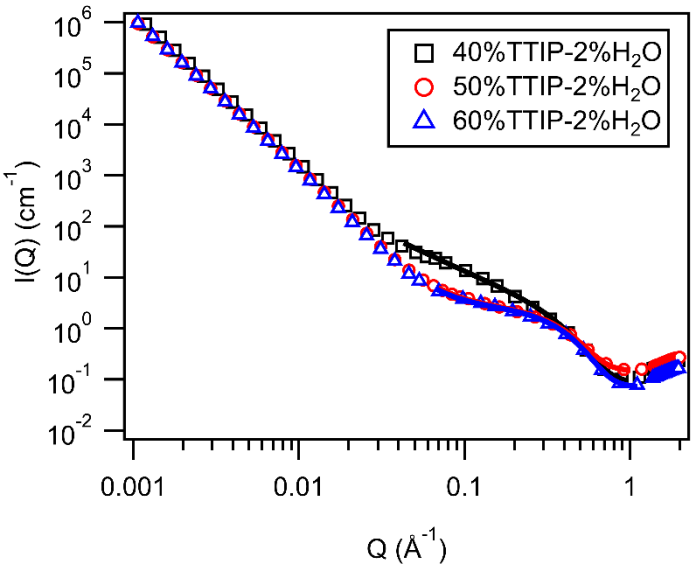

Figure 3.3: The scattering graphs and their fit of TTIP-H_2O membranes with different compositions.

Table 3.1: The Fit Results of TTIP-H_2O Membranes with Different Compositions

Sol-gel solution compositions	Pore volume fraction	Pore radius (Å)	Fractal dimension	Radius width
40% TTIP-2% H_2O-58% EtOH	0.0317	4.12	1.68	0.300
50% TTIP-2% H_2O-48% EtOH	0.0389	4.48	2.98	0.231
60% TTIP-2% H_2O-38% EtOH	0.0383	4.51	2.99	0.229

3.1.2 *The Structure Information of Membranes Made from TTIP and TEOS*

Figure 3.4 shows the surface images and cross-sectional images of the membrane made from TTIP and TEOS (TTIP-TEOS membrane). The cross-section images show that the structures of the

titania and silica inside the membrane are similar to those of the TTIP-H_2O membrane. A xerogel film also forms on the top of the TTIP-TEOS membrane but with some particle aggregating on the xerogel film. These particles could be silica that is unable to bind with the titania.

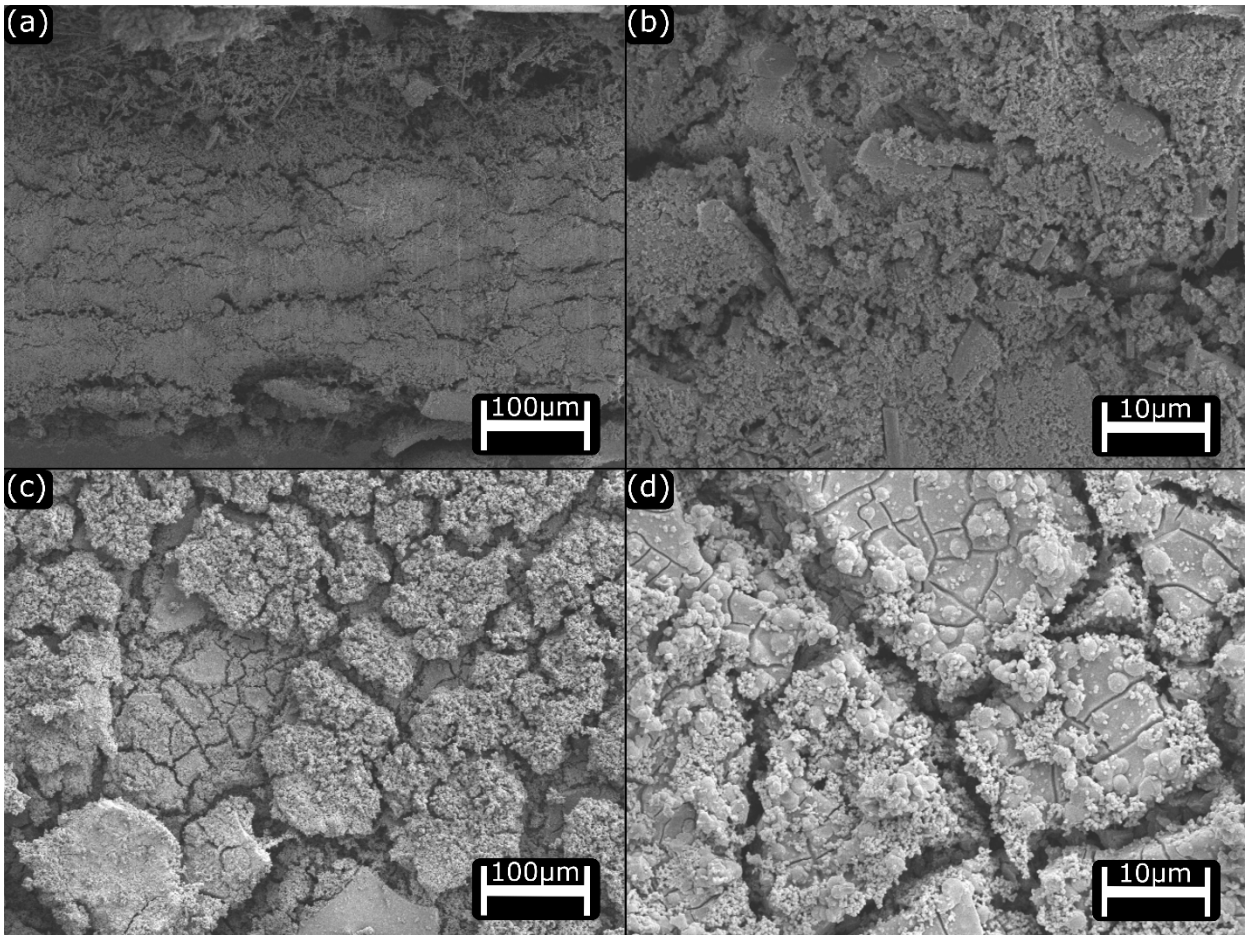

Figure 3.4: The SEM images of the membrane made from 38% TTIP, 2% TEOS and 60% EtOH. Cross-sectional images in (a) 100 μm scale and in (b) 10 μm scale; Surface images in (c) 100 μm scale and in (d) 10 μm scale.

The scattering graphs of membranes with different compositions of TTIP and TEOS and their fit are shown in Figure 3.5. The fit results obtained from fractal model are shown in Table 3.2. These three membranes show similar fit results of the pore radius and the fractal dimension. As the concentration of TTIP increases in the precursor solution, the pore volume fraction increases.

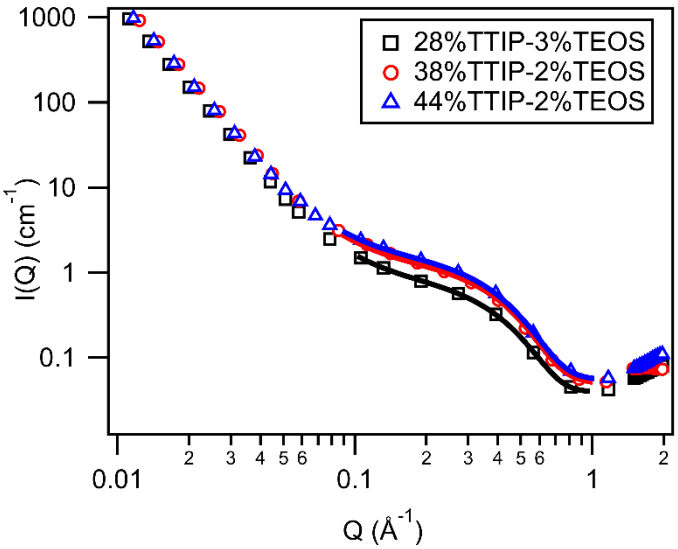

Figure 3.5: The scattering graphs and their fit of TTIP-TEOS membranes with different compositions.

Table 3.2: The Fit Results of TTIP-TEOS Membranes with Different Compositions

Sol-gel solution compositions	Pore volume fraction	Pore radius (Å)	Fractal dimension	Radius width
28% TTIP-3% TEOS-69% EtOH	0.0129	4.71	2.96	0.191
38% TTIP-2% TEOS-60% EtOH	0.0212	4.50	2.97	0.229
44% TTIP-2% TEOS-54% EtOH	0.0242	4.50	2.98	0.215

3.2 The Structure Information of Sintered Titania Membranes

Titania membranes show the problem that membranes cannot survive in 3M hydrochloric acid. The titania coating seems to be washed out and blank silica paper is left after they are soaked in 3M HCl for a day. However, titania should be insoluble in hydrochloric acid [17]. The problem may be caused by the formation of small titania particles instead of a large xerogel inside the membranes. In order to solve this problem, titania membranes are sintered to form a stronger structure. After sintering, membranes become very brittle.

3.2.1 *The Structure Information of Sintered Membranes Made from TTIP and Water*

The scattering graphs and fit results of TTIP-H_2O membranes sintered at 450℃ are shown below. The scattering graphs and fit results of the membrane with 50% of TTIP are similar to those of the membrane with 60% of TTIP. The pore radius and the pore volume fraction change as the composition changes. The fractal dimension is close to 3.

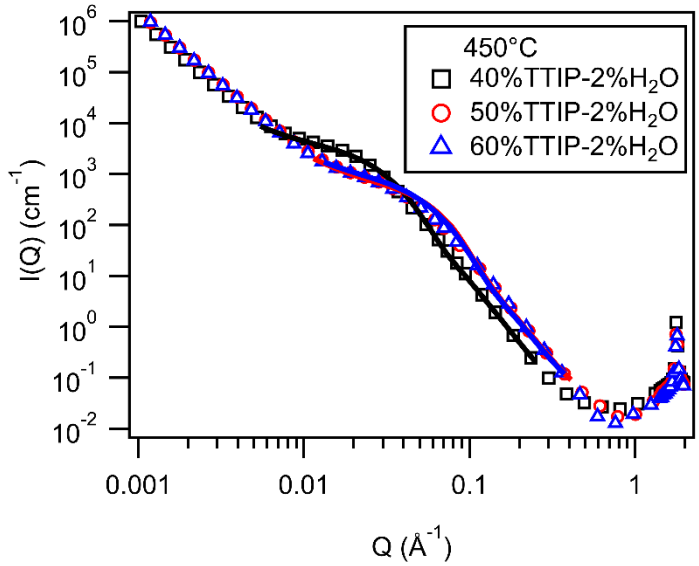

Figure 3.6: The scattering graphs and their fit of TTIP-H_2O membranes sintered at 450℃ with different compositions.

Table 3.3: The Fit Results of TTIP-H_2O Membranes Sintered at 450 ℃ with Different Compositions

Sol-gel solution compositions	Pore volume fraction	Pore radius (Å)	Fractal dimension	Radius width
Being sintered at 450℃				
28% TTIP-3% TEOS-69% EtOH	0.029	51.5	2.94	0.300
38% TTIP-2% TEOS-60% EtOH	0.037	27.6	2.93	0.300
44% TTIP-2% TEOS-54% EtOH	0.037	28.0	2.94	0.298

3.2.2 *The Structure Information of Sintered Membranes Made from TTIP and TEOS*

After being sintered at 450℃, the TTIP-TEOS membrane shows totally different structures under SEM. The xerogel film disappears, and some cylindrical particles appear, which are illustrated more clearly in cross-sectional images. There are clearly other particles also aggregating on the cylindrical particles.

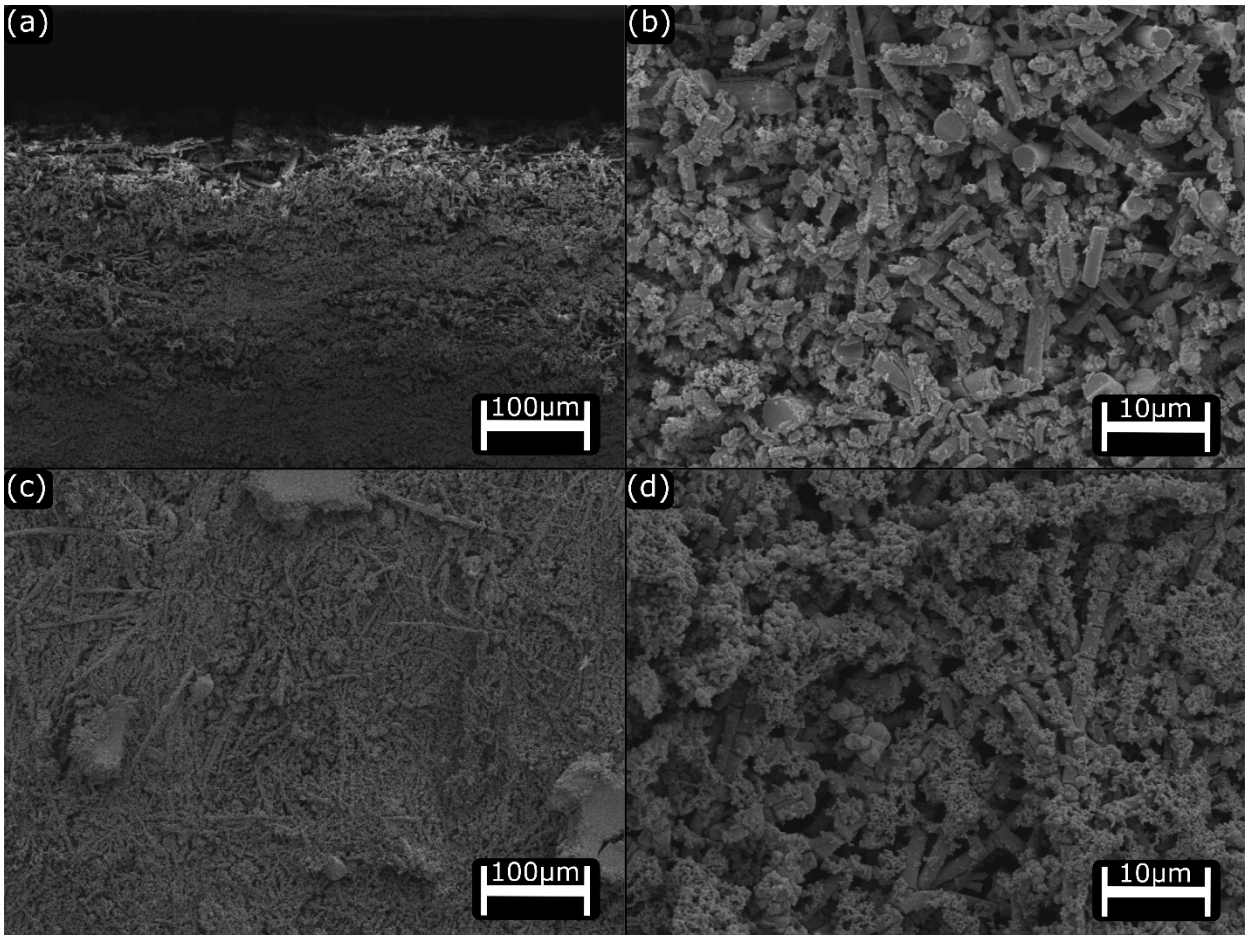

Figure 3.7: The SEM images of the membrane made from 38% TTIP, 2% TEOS and 60% EtOH and sintered at 450℃. Cross-sectional images in (a) 100 μm scale and in (b) 10 μm scale; Surface images in (c) 100 μm scale and in (d) 10 μm scale.

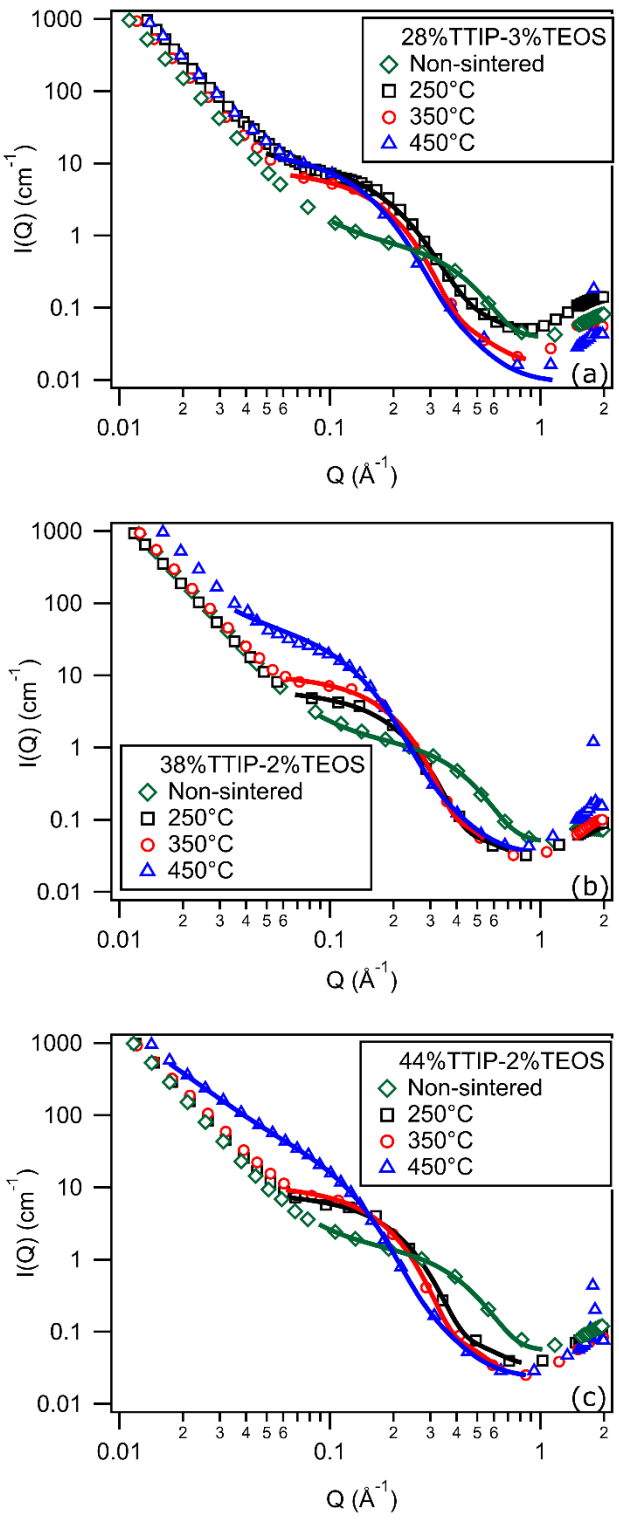

Figure 3.8: The scattering graphs and fit results of membranes sintered at different temperatures with different compositions of TTIP and TEOS. Membranes with the composition of (a) 28%

TTIP, 3% TEOS, and 69% EtOH (b) 38% TTIP, 2% TEOS, and 60% EtOH, and (c) 44% TTIP, 2% TEOS and 54% EtOH.

The figures above are the scattering figures of TTIP-TEOS membranes after sintering, and their fit also are included. The fit results of every parameter are shown in Table 3.4. Generally, as sintering temperature increases, the pore radius of membranes with the same composition will increase, but the volume fraction does not reveal a clear trend. The fractal dimension is close to 3.

Table 3.4: The Fit Results of Membranes Sintered at Different Temperatures with Different Compositions

Sintering temperature	Pore volume fraction	Pore radius (Å)	Fractal dimension	Radius width
28% TTIP-3% TEOS-69% EtOH				
250℃	0.0166	7.88	2.98	0.300
350℃	0.0109	9.60	3.00	0.232
450℃	0.0103	10.2	3.00	0.300
38% TTIP-2% TEOS 60%EtOH				
250℃	0.0117	8.94	3.00	0.212
350℃	0.0234	10.2	3.00	0.186
450℃	0.0206	12.1	2.94	0.300
44% TTIP-2% TEOS-54% EtOH				
250℃	0.0149	9.06	3.00	0.211
350℃	0.0131	10.5	3.00	0.206
450℃	0.0122	13.7	2.68	0.300

3.3 The Structure Information of Membranes Made from Ludox® CL

Figure 3.9 shows the SEM images of a membrane made with Ludox® CL and titania. The cross-sectional images don't show much difference from TTIP-H_2O membranes. Surface images show that a xerogel film forms, but part of them disappear, and inner structures are exposed. Titania might be difficult to combine with silica paper after it is coated with Ludox® CL. Figure 3.9 (d) should be the image of the xerogel film left on the membrane.

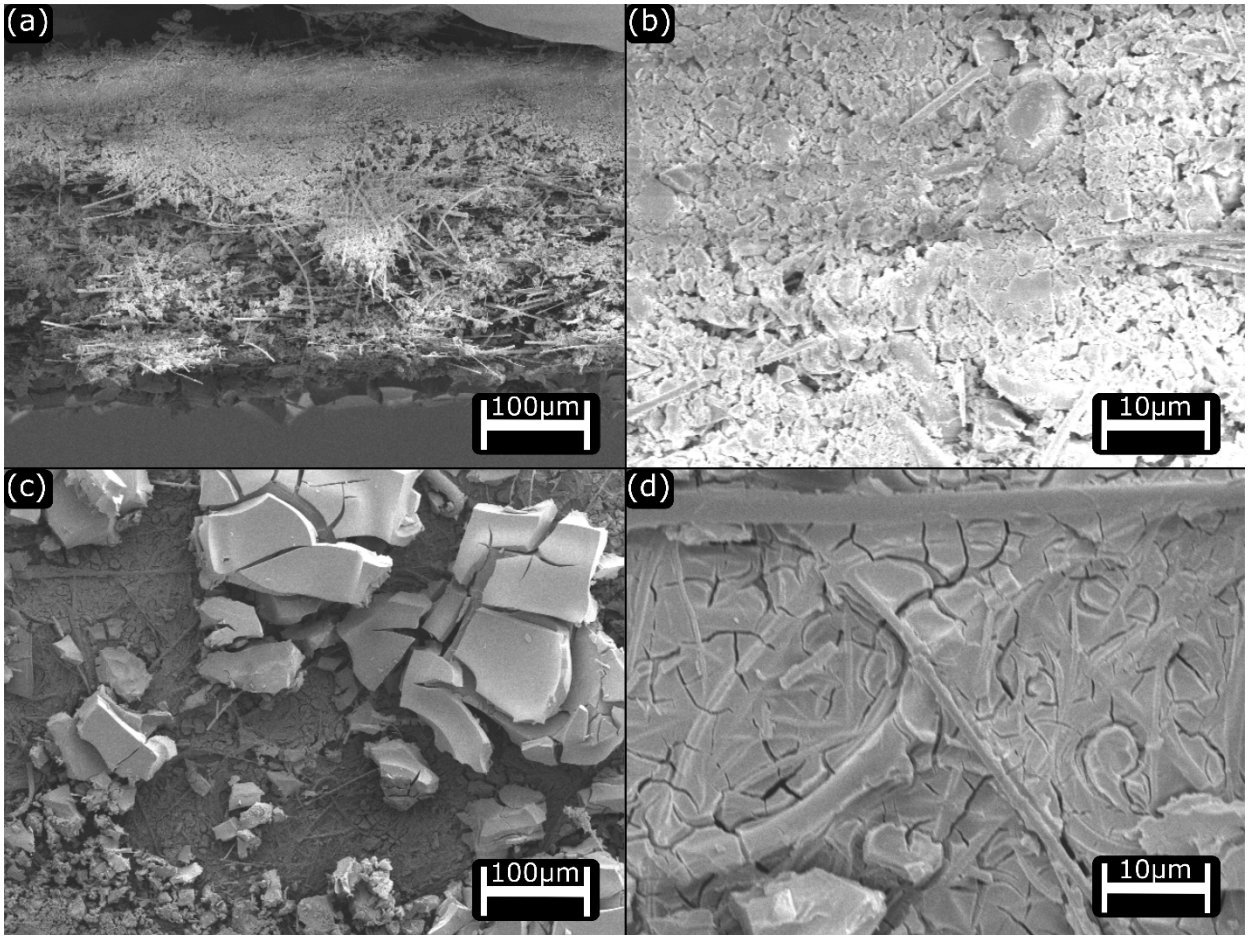

Figure 3.9: The SEM images of the membrane made from Ludox® CL and titania. Cross-sectional images in (a) 100 µm scale and in (b) 10 µm scale; Surface images in (c) 100 µm scale and in (d) 10 µm scale.

The SEM images of the membrane made from Ludox® CL and silica shows different structures from the membranes shown before. The surface images also illustrate that a xerogel film forms on the top of the membrane. However, the cross-sectional images show completely different structures. More uniform and compact structures form.

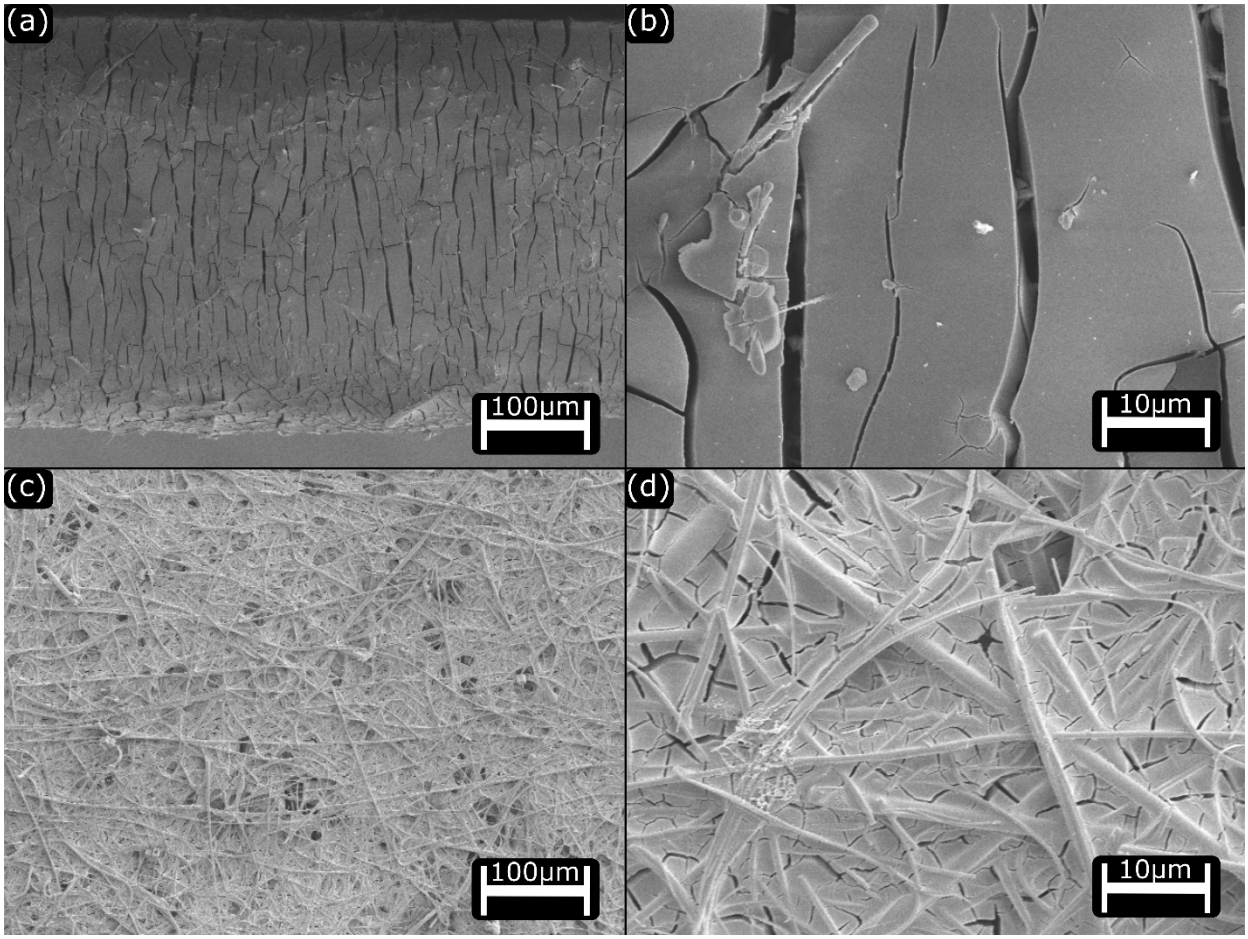

Figure 3.10 The SEM images of the membrane made from Ludox® CL and silica. Cross-sectional images in (a) 100 μm scale and in (b) 10 μm scale; Surface images in (c) 100 μm scale and in (d) 10 μm scale.

3.4 THE RESULTS OF PERMEABILITY TESTS

Table 3.5 shows permeability test results of membranes sintered at 450 ℃ with different compositions. The samples with 44% of TTIP show quite different permeability test results from each other. Only one permeability test is successfully performed on the membrane with lower compositions of TTIP. Thus, their permeability test results might not represent their real performance. In permeability tests, lower permeability means better performance to block Fe^{3+}. These membranes show worse permeability performance than that of Nafion membrane (~1.4e-4 cm/min [10]), and as the composition of TTIP increases, their permeability performance is better.

The membranes made from Ludox® CL and silica has much better permeability performance, and the results are close to the performance of Nafion.

Table 3.5: Permeability Test Results of Membranes Sintered at 450℃

Sample Name	Extrinsic permeability of Fe^{3+} (cm/min)
44% TTIP-2% TEOS-54% EtOH-450℃	
Trial 1	2.7e-4
Trial 2	8.8e-4
Trial 3	1.8e-3
44% TTIP-2% TEOS-54% EtOH-450℃ mean	9.8e-4
38% TTIP-2% TEOS-60% EtOH-450℃	4.7e-3
28% TTIP-3% TEOS-69% EtOH-450℃	1.4e-2

Table 3.6: Permeability Test Results of Membranes Made from Ludox® CL and Silica

Sample Name	Extrinsic permeability of Fe^{3+} (cm/min)
Ludox® CL+40% TEOS-2% H_2O-58% EtOH	
Trial 1	1.1e-4
Trial 2	2.5e-4
Trial 3	2.9e-3
Mean	2.2e-4

3.5 The Results of Stability Tests

Figure 3.11 compares nanostructures of samples before being soaked in KOH and after being soaked in KOH. If the chemicals in the sample are soluble in KOH, the nanostructures will change, and their scattering graphs will show different features. The scattering graphs of blank cellulose paper and Ludox® CL almost keep the same while that of titania changes dramatically.

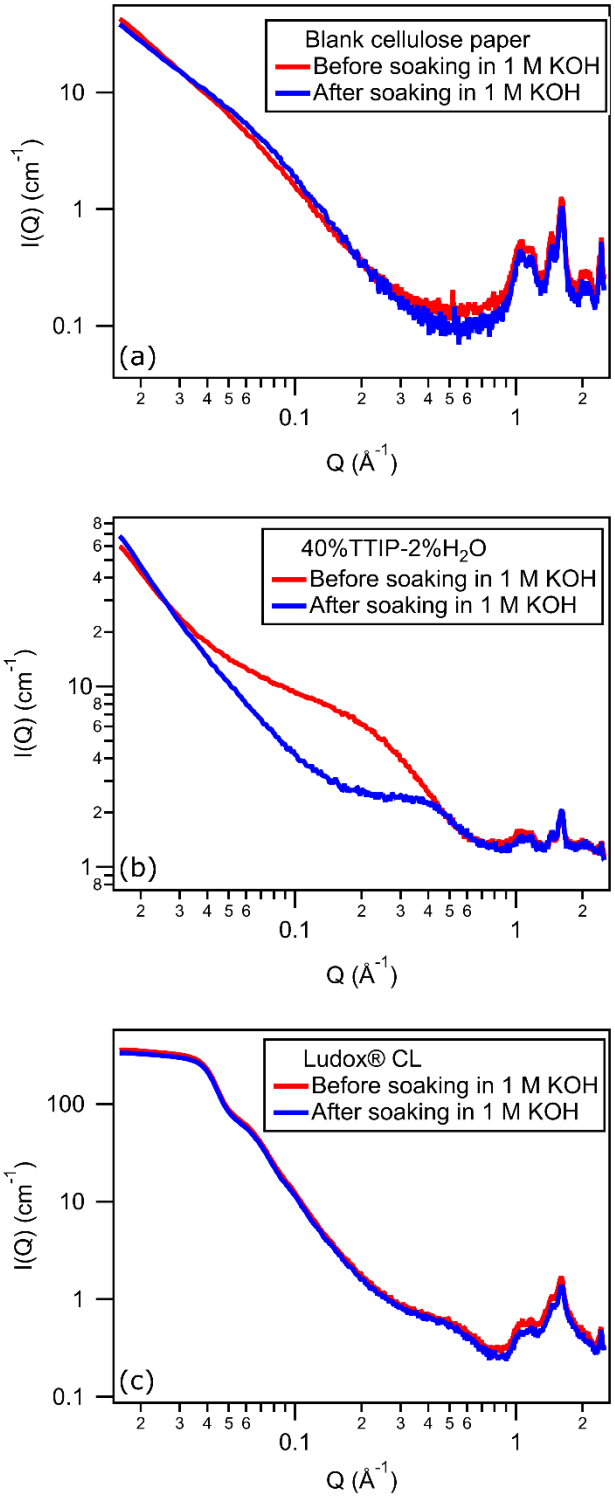

Figure 3.11: The scattering graphs of samples before being soaked in base and after being soaked in base. (a) Blank cellulose paper; (b) Cellulose paper coated with titania; (c) Cellulose paper coated with Ludox® CL.

Chapter 4. DISCUSSION

Interestingly, after being sintered at 450℃, some organized peaks show up in high q range for both TTIP-H_2O membranes and TTIP-TEOS membranes. However, these peaks don't appear for membranes sintered at lower temperatures or without sintering, except for the membrane with the composition of 44% TTIP and 2% TEOS. Figure 4.1 illustrates this phenomenon. Crystal structures might form after being sintered at high temperature. The cylindrical particles shown in Figure 3.7 should be titania crystals.

Titania has different crystal structures like anatase and rutile. In order to figure out which crystal structures form after sintering, the WAXS part of the graph is analyzed using standard diffraction units (2θ). Figure 4.2 shows the comparison between the membrane sintered at 450℃ and the titania sample containing anatase, brookite, and rutile. The diffraction image of the membrane sintered at 450℃ shows the feature peaks of anatase, so an anatase crystal forms after the membrane is sintered at 450℃.

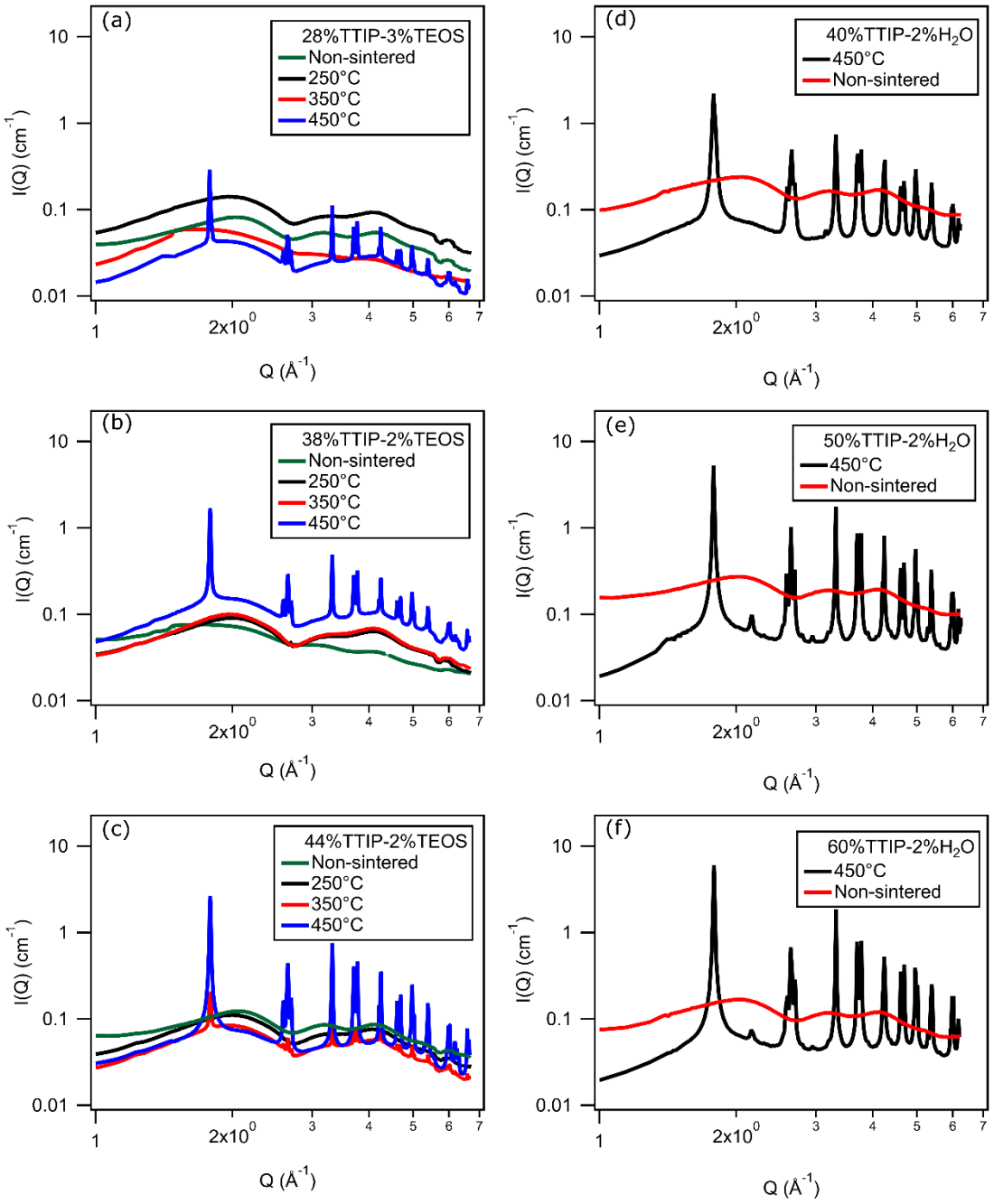

Figure 4.1: The scattering graphs in WAXS region of membranes sintered at different temperatures with different compositions. Membranes with the composition of (a) 28% TTIP, 3% TEOS, and 69% EtOH, (b) 38% TTIP, 2% TEOS, and 60% EtOH, (c) 44% TTIP, 2% TEOS and 54% EtOH, (d) 40% TTIP, 2% H_2O, and 58% EtOH, (e) 50% TTIP, 2% H_2O, and 48% EtOH, and (f) 60% TTIP, 2% H_2O, and 38% EtOH.

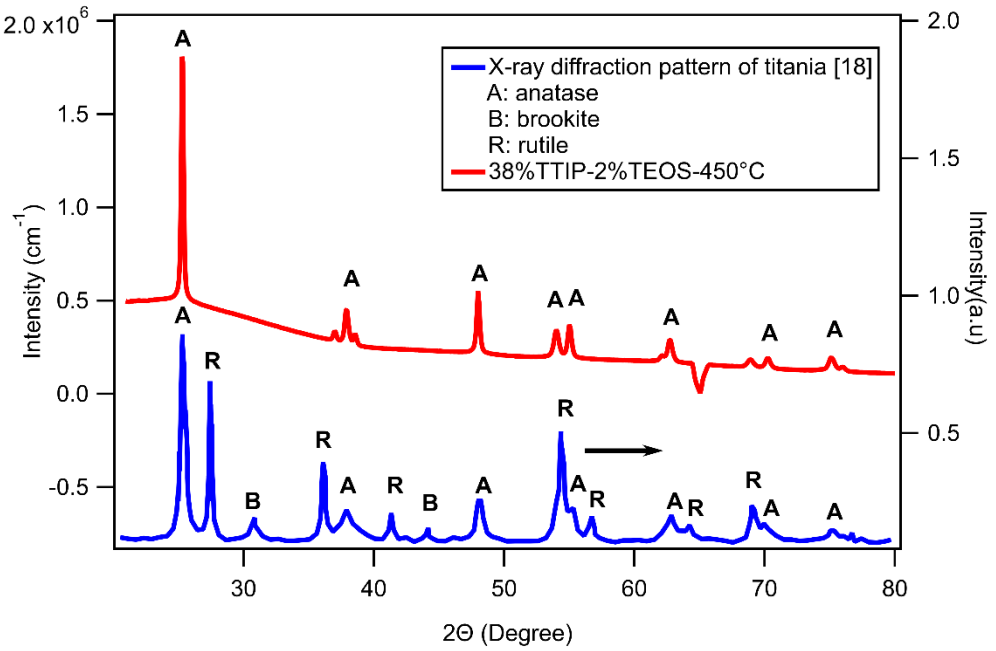

Figure 4.2: X-ray diffraction pattern of the membrane sintered at 450℃ and the titania sample containing anatase, brookite, and rutile [18].

The cross-sectional images of non-sintered TTIP-H_2O membranes and TTIP-TEOS membranes show similar structure while there is more aggregation of spherical particles for TTIP-TEOS membranes in surface images. These spherical particles should be silica. These two types of titania membranes have similar size of the pore radius before sintering. However, after being sintered at 450℃, the pore radius of TTIP- H_2O membrane is almost as twice large as that of TTIP-TEOS membrane. Silica might help the membrane to maintain small pore size during sintering.

For membranes sintered at different temperatures with different compositions of TTIP and TEOS, there is a clear relationship between the pore radius and the temperature. The pore radius becomes larger as the temperature increases. At higher sintering temperatures, the residual solvent would evaporate faster, which may cause larger pore radii. Interestingly, the composition of the precursor solution does not affect the pore radius a lot when sintering temperatures are the same. The relationship among the pore volume fraction, solution compositions, and sintering

temperatures does not show clearly. The pore volume fraction might also be influenced by other factors, like how much the precursor solution was coated in the substrate and the humidity of the air when the membrane is dried out.

In permeability tests, the samples with 44% of TTIP show quite different permeability test results from each other, and this may be caused by the edge addition process. The membrane becomes very brittle after sintering. The polymer edge addition process might cause some unknown cracks, which can affect the permeability test results. Membranes sintered at 450℃ show better permeability performance as the composition of TTIP increases. The membrane may contain more titania if the TTIP composition is higher in the precursor solution. The membrane may carry more positive charges under acidic condition and show better permeability performance. Ideally, the smaller pore radius is better to prevent the crossover of electrolyte. Therefore, the membrane sintered at lower temperature with higher composition of TTIP is preferred.

The membrane made from Ludox® CL and silica shows totally different structures in cross-sectional images. The structures are more compact and uniform. Large Ludox® CL particles might provide stronger resistance to the tensile stress causing cracks. Thus, the surface images show a xerogel film with less cracks. Ludox® CL would carry positive charges under natural condition because of the layer of alumina. Silica would carry negative charges under natural condition. The attraction of opposite charges might help silica particles to combine with Ludox® CL to form a uniform structure. These membranes also show better permeability performance than sintered TTIP-TEOS membranes.

In stability tests, the scattering graph of blank cellulose paper changes slightly in low q range after soaking in base, but the feature peaks in high q range stay the same. Thus, cellulose paper is stable in KOH, and can be the substrate of the membrane used in alkaline-based ORFBs. The

feature peak of the titania sample moves to higher q after soaking in KOH, which means that titania might dissolve in KOH or might react with KOH. The titania sample might survive in KOH after sintering. The scattering graph of Ludox® CL stays the same after the stability test. The alumina layer of Ludox® CL is stable in KOH, and alumina can be the membrane materials applied in alkaline-based ORFBs.

Chapter 5. CONCLUSION

Xerogel networks with cracks show on the top of membranes by hydrolyzing TTIP and TEOS. However, titania membranes cannot survive in 3 M HCl. After being sintered, titania membranes can work in 3 M HCl but lose the xerogel network. As sintering temperature increases, the pore radius of TTIP-TEOS membrane increases, and an anatase crystal structure forms at the sintering temperature of 450℃. The sintered TTIP-TEOS membrane shows much worse permeability performance than Nafion membranes. Thus, titania might not be the proper membrane materials used for the anion exchange membrane in RFBs. The xerogel film of Ludox membranes show smaller cracks in surface images, so Ludox® CL helps to reduce the size of cracks. The alumina layer of Ludox® CL is stable in 1 M KOH. Therefore, alumina might be a promising membrane material for use in alkaline-based ORFBs.

Chapter 6. FUTURE PLAN

Titania membranes might be improved by decreasing the rate of hydrolyzation to form uniform structures with less cracks. Ethanol can be replaced with 2-methoxy ethanol, and1,5-pentanediol can be mixed with ethanol to stabilize the titania precursor. Alumina is a promising material that could be used in alkaline-based ORFBs. Cellulose paper coated with alumina precursor can be further studied. Alumina can be prepared by hydrolyzing aluminum s-butoxide. Ludox® CL can also be added to the alumina membrane to reduce the amount and the size of cracks.

APPENDIX A

Titania particles aggregate in membranes, but the mechanism for particle aggregation is unknown. Thus, a fractal model is picked to fit the scattering data. Scattering data contain USAXS, SAXS, WAXS parts, and it is hard fit such a wide q range with a single model, so scattering data are fit using a combined model (Guinier-Porod model plus fractal model). However, the combined model did not provide more meaningful information than the single fractal model and it just added uncertainty in fitting parameters. Figure A.1 shows that, compared with blank silica paper, a new feature appears in the SAXS region after coating. Thus, the fitting process is simplified to fitting this SAXS region with the simple fractal model.

The fractal model is calculated based on Equation A.1:

$$I(q) = \phi V_{block}(\rho_{block} - \rho_{solvent})^2 P(q) S(q) + background \quad \text{(A.1)}$$

where ϕ is the volume fraction of building blocks, V_{block} is the volume of a single building block, ρ_{block} is the scattering length density of building blocks, $\rho_{solvent}$ is the scattering length density of the solvent, $P(q)$ is the form factor, and $S(q)$ is the structure factor [19], [20]. The volume of a single building block is calculated by the sphere volume formula. The form factor and the structure factor are obtained by Equation A.2 and A.3:

$$P(q) = F(qR_0)^2, F(q) = \frac{3(sinx - xcosx)}{x^3} \quad \text{(A.2)}$$

$$S(q) = 1 + \frac{D_f \Gamma(D_f - 1)}{[1 + 1/(q\xi)^2]^{(D_f-1)/2}} \frac{sin\,[(D_f - 1)tan^{-1}(q\xi)]}{(qR_0)^{D_f}} \quad \text{(A.3)}$$

where R_0 is the radius of building blocks, D_f is the fractal dimension, and ξ is the cluster correlation length [19], [20].

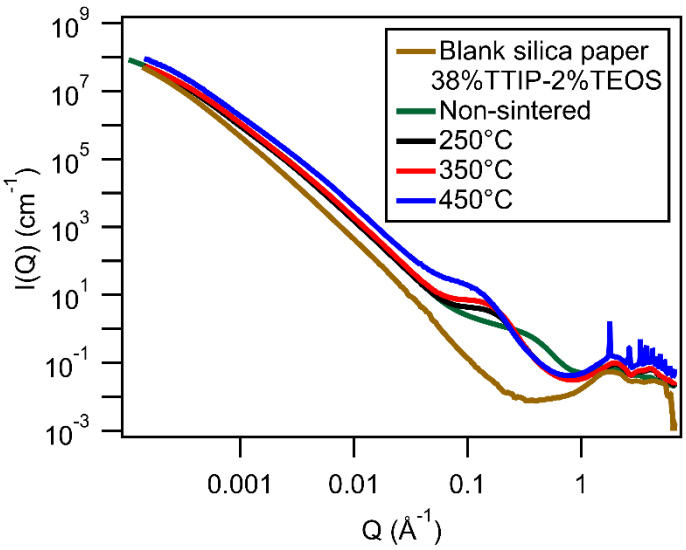

Figure A.1: Scattering graphs of blank silica paper and titania membranes.

Table A.1 illustrates the value of every parameter shown in the fractal model of SasView[19]. Some of them are fixed to certain number, and some of them are fit by the model. Core length is the largest dimension of the fractal aggregate, which should be very large relative to the radius of building blocks. Thus, core length is set to an arbitrary large number. Scattering length density (SLD) of the block is the SLD of titania, and SLD of the solvent is that of air. The fit results of the volume fraction are always less than 5% for every membrane, but the volume fraction of titania should be much higher than this, so it should be the volume fraction of pores, and the radius of blocks should be the pore radius. Air is the building block particle, and titania is the solvent. Since the scattering contrast is proportional to the difference in SLD squared, the reverse of SLD does not affect fit results. The radius width represents the size polydispersity of pores, which is the ratio of standard deviation to median value of the distribution. Radius width is calculated based on lognormal distribution.

Table A.1: The Parameters in Fractal Model and Their Values [19]

Parameter	Value
Scale	1
Background	Fit
Volume fraction	Fit
Radius	Fit
Fractal dimension	Fit
Core length	10000 (Å)
SLD block	30.8e-6 ($Å^{-2}$)
SLD solvent	0 ($Å^{-2}$)
Radius width	Fit

APPENDIX B

The principle of the permeability test is described in *Analysis of Transport Phenomenon* and is shown below [21]. The diffusion of Fe^{3+} in the membrane is assumed to be pseudo steady state, so Fick's law can be written as

$$0 = D\frac{\partial^2 C}{\partial x^2} \tag{B.1}$$

where C is the concentration of Fe^{3+} in the membrane, and D is diffusion coefficient. The concentration at the two ends of the membrane are:

$$C(0,t) = KC_1(t) \tag{B.2}$$

$$C(L,t) = KC_2(t) \tag{B.3}$$

where C_1 is the concentration of Fe^{3+} in the $FeCl_3$ cell, C_2 is the concentration of Fe^{3+} in the $AlCl_3$ cell. K is the membrane/external partition coefficient. Equation B.1 can be solved to obtain:

$$C(x,t) = KC_1(t) + K[C_2(t) - C_1(t)]\frac{x}{L} \tag{B.4}$$

where L is the thickness of the membrane. The flux of Fe^3 at two ends of the membrane can be obtained by plugging Equation B.3 into equation below:

$$N_x(0,t) = N_x(L,t) = -D\frac{\partial C}{\partial x} = \frac{DK[C_1(t) - C_2(t)]}{L} \tag{B.5}$$

The governing equations of two cells and their initial concentrations of Fe^{3+} are:

$$\frac{dC_1}{dt} = -\frac{A}{V}N_x(0,t) = -\frac{ADK}{VL}\big(C_1(t) - C_2(t)\big), C_1(0) = C_0 \tag{B.6}$$

$$\frac{dC_2}{dt} = +\frac{A}{V}N_x(L,t) = +\frac{ADK}{VL}\big(C_1(t) - C_2(t)\big), C_2(0) = 0 \tag{B.7}$$

where C_0 is the initial concentration of Fe^{3+} in $FeCl_3$ cell. Solve Equation B.6 and B.7 simultaneously to obtain the concentration function of Fe^{3+} in $AlCl_3$ cell.

$$C_2(t) = \frac{C_o}{2}(1 - e^{-\frac{t}{\tau}}) \tag{B.8}$$

τ is

$$\tau = \frac{VL}{2ADK} \tag{B.9}$$

where A is the contact area of the membrane, and V is the solution volume in either cell. The extrinsic permeability of Fe^{3+} can be calculated by equation below.

$$p = \frac{DK}{L} = \frac{V}{2A\tau} \tag{B.10}$$

In the permeability test, the concentration function of Fe^{3+} in $AlCl_3$ cell is obtained by measuring the absorbance of Fe^{3+} after each time interval. The absorbance is converted to the concentration using Beer's law. Concentrations are plotted versus time as figure shown below. It takes some time for the membrane to reach pseudo steady state. When the diffusion of Fe^{3+} reaches pseudo steady state, the rate of concentration change will increase. Thus, Equation B.8 is used to fit second part of data points to obtain τ. The extrinsic permeability of Fe^{3+} can be calculated using Equation B.10.

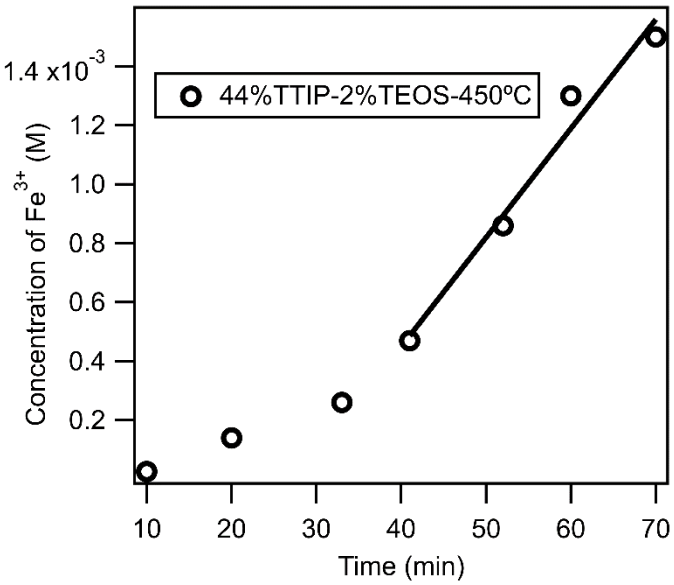

Figure B.1: The concentration data collected in the permeability test of the membrane sintered at 450 ℃ with the composition of 44% TTIP, 2%TEOS, and 54%EtOH.

BIBLIOGRAPHY

[1] A. Z. Weber, M. M. Mench, J. P. Meyers, P. N. Ross, J. T. Gostick, and Q. Liu, "Redox flow batteries: A review," *J. Appl. Electrochem.*, vol. 41, no. 10, pp. 1137–1164, 2011.

[2] US Department of Energy, "Advanced Materials and Devices for Stationary Electrical Energy Storage Applications," *Energy*, vol. 44, no. December, pp. 259–281, 2010.

[3] M. Zhang, M. Moore, J. S. Watson, T. A. Zawodzinski, and R. M. Counce, "Capital Cost Sensitivity Analysis of an All-Vanadium Redox-Flow Battery," *J. Electrochem. Soc.*, vol. 159, no. 8, pp. A1183–A1188, 2012.

[4] W. Wang, Q. Luo, B. Li, X. Wei, L. Li, and Z. Yang, "Recent progress in redox flow battery research and development," *Adv. Funct. Mater.*, vol. 23, no. 8, pp. 970–986, 2013.

[5] H. Chen, G. Cong, and Y. C. Lu, "Recent progress in organic redox flow batteries: Active materials, electrolytes and membranes," *J. Energy Chem.*, 2018.

[6] B. Schwenzer, J. Zhang, S. Kim, L. Li, J. Liu, and Z. Yang, "Membrane development for vanadium redox flow batteries," *ChemSusChem*, vol. 4, no. 10, pp. 1388–1406, 2011.

[7] J. Xi, Z. Wu, X. Qiu, and L. Chen, "Nafion/SiO2hybrid membrane for vanadium redox flow battery," *J. Power Sources*, vol. 166, no. 2, pp. 531–536, 2007.

[8] H. Schmidt, "Chemistry of material preparation by the sol-gel process," *J. Non. Cryst. Solids*, vol. 100, no. 1–3, pp. 51–64, 1988.

[9] L. L. Hench and J. K. West, "The Sol-Gel Process," *Chem. Rev.*, vol. 90, no. 1, pp. 33–72, 1990.

[10] G. M, Newbloom., A. West, R. Kastillani, C. Wei, J. Rodriguez, and L. Pozzo D., "Durable Sol-Gel Ceramic Membranes and Method of Preparation," 62613712, 2018.

[11] J. Nawrocki *et al.*, "Part II. Chromatography using ultra-stable metal oxide-based stationary phases for HPLC," *J. Chromatogr. A*, vol. 1028, no. 1, pp. 31–62, 2004.

[12] M. A. Anderson, "Titania and alumina ceramic membranes," *J. Memb. Sci.*, vol. 39, no. 3, pp. 243–258, 1988.

[13] S. Rezgui and B. C. Gates, "Sol-Gel Synthesis of Alumina in the Presence of Acetic Acid: Distinguishing Gels and Gelatinous Precipitates by NMR Spectroscopy," *Chem. Mater.*, vol. 6, no. 12, pp. 2386–2389, 1994.

[14] C. J. Brinker *et al.*, "Sol-gel strategies for controlled porosity inorganic materials," *J. Memb. Sci.*, vol. 94, no. 1, pp. 85–102, 1994.

[15] H. Schnablegger and Y. Singh, "The SAXS Guide," *Ant. Paar*, pp. 1–99, 2011.

[16] H. Kozuka, S. Takenaka, H. Tokita, T. Hirano, Y. Higashi, and T. Hamatani, “Stress and cracks in gel-derived ceramic coatings and thick film formation,” *J. Sol-Gel Sci. Technol.*, vol. 26, no. 1–3, pp. 681–686, 2003.

[17] JEFCA (The Joint FAO/WHO Expert Committee on Food Additives), “Titanium Dioxide,” *FAO JECFA Monogr. 13 Prep. 76th JECFA*, vol. 13, pp. 1–4, 2012.

[18] H. Esteban Benito, T. Del Ángel Sánchez, R. García Alamilla, J. M. Hernández Enríquez, G. Sandoval Robles, and F. Paraguay Delgado, “Synthesis and physicochemical characterization of titanium oxide and sulfated titanium oxide obtained by thermal hydrolysis of titanium tetrachloride,” *Brazilian J. Chem. Eng.*, vol. 31, no. 3, pp. 737–745, 2014.

[19] P. Bulter, M. Doucet, A. Jackson, and S. King, “Sasview for Small Angle Scattering Analysis.” [Online]. Available: https://www.sasview.org/.

[20] J. Teixeira, “Small-angle scattering by fractal systems,” *J. Appl. Crystallogr.*, vol. 21, no. 6, pp. 781–785, 1988.

[21] W. Deen, *Abalysis of Transport Phenomena*, Second. Oxford University Press, 2012.